STRENGTHENING MECHANISMS AND FRACTURE BEHAVIOR OF 7072Al/Al_2O_3 METAL MATRIX COMPOSITES

A. CHENNAKESAVA REDDY

Department of Mechanical Engineering
JNTUH College of Engineering
Hyderabad – 500085, Andhra Pradesh, India
dr_acreddy@yahoo.com

ESSA ZITOUN

Department of Mechanical Engineering
University College of Engineering, Osmania University
Hyderabad, Andhra Pradesh, India

Abstract:

The use of gravity die casting process has been studied to fabricate 7072/Al_2O_3 metal matrix composites. The mechanical properties have been evaluated. The composites having volume fraction of 20% alumina gave the maximum values of flexural, fracture and yield strengths. The hardness increased with the increase of alumina addition to 7072 matrix alloy. The strengthening mechanisms were largely governed by the strain hardening and by the change in grain size. The ductility decreased with the increase in volume fraction of Al_2O_3 in the composite. Clustering/agglomeration of silicon carbide particulates was observed in some of the tensile test specimens. The coarse and connected $MgZn_2$ phases were precipitated along the grain boundaries. $Mg_{17}Al_{12}$ intermetallic phase was also revealed at the grain boundary junctions. Al_7Cu_2Fe were clustered in bands in the composite. The tensile fracture was governed by the ductile and brittle behaviors because of void nucleation at particle/matrix interfaces, decohesion of particles from the matrix and particle/cluster cracking.

Keywords: gravity die casting; 7072, alumina; fracture strength; flexural strength; hardness; ductility.

1. Introduction

Metal matrix composites (MMCs) reinforced by carbides and oxides have been successfully fabricated by casting methods. Hunt et al (1991) and Chawla (1997) have expressed that the aluminum alloy based metal matrix composites are attractive and viable candidate for automobile and aerospace applications. The mechanical properties of aluminum alloys reinforced with ceramic particulates are known to be influenced by the particle size and the volume fraction. Arsenault (1984) and Wang and Zhang (1991) found that yield strength and tensile strength tend to increase, and toughness and ductility decrease with increasing volume fraction of particulate or decreasing particle size.

For optimum strength, the second-phase dispersion strengthened particles must be fine and the interparticular spacing small. Upon the application of a stress at room temperature, dislocations are captured and pushed through the gaps between these particles. Dutta and Bourell (1990) have stated that the high density of dislocations both at and near the reinforcement/matrix interfaces is aroused as a result of the mismatch in the coefficient of thermal expansion between the SiC particle and the aluminium alloy matrix. Clustering leads to a non-homogeneous response and lower macroscopic mechanical properties. Lloyd (1991) and Nair (1985) revealed that the particle clusters act as crack or decohesion nucleation sites at stresses lower than the matrix yield strength, causing the MMC to fail at unpredictable low stress levels. Possible reasons resulting in particle clustering are chemical bonding, surface energy reduction or particle segregation as pointed out by Youssef et al (2005). Srivatsan et al (1991) have declared that among all the liquid-state processes, stir-casting technology is considered to be the most potential method for engineering applications in terms of production capacity and cost efficiency. Zhou and Xu (1997) have developed a two-step stirring process for homogeneous particle distribution to prepare particulate metal matrix composites.

The motivation for this work was to study the influence of microstructure (as-cast and heat-treatment conditions), volume fraction of alumina (Al_2O_3) reinforcement on the tensile, flexural and fracture behavior of 7072 aluminium alloy metal matrix composite reinforced with Al_2O_3 particles.

2. Experimental Procedure

The matrix alloy is 7072 Al. The volume fractions (V_f) of Al_2O_3 particulate reinforcement are 10%, 20% and 30%. The particle size of Al_2O_3 reinforcement is 10 μm.

2.1. Preparation of melt and metal matrix composites

Al alloys were melted in a resistance furnace. The crucibles were made of graphite. The melting losses of alloy constituents were taken into account while preparing the charge. The charge was fluxed with coverall to prevent dressing. The molten alloy was degasified by tetrachlorethane (in solid form). The crucible was taken out of the furnace and modified with sodium. Then the liquid melt was allowed to cool down just below the liquidus temperature to bring the melt semi solid state. At this stage, the preheated (1000^0C for 1 hour) Al_2O_3 particles were added to the liquid melt. The molten 7072 alloy and Al_2O_3 particles are thoroughly stirred manually. After sufficient manual stirring, the semi-solid liquid melt was reheated to a fully liquid state in the resistance furnace followed by automatic mechanical stirring using a mixer to make the melt homogenous for about 15 minutes at 200 rpm. The temperature of the melt was measured using a dip type thermocouple. The dross removed melt was finally gravity poured into the preheated cast iron mould.

2.2. Heat-treatment

Prior to machining of the composite samples, a solution treatment was applied at 550^0 C for 15 min quenched in cold water, and aged at 150^0C for 100 hours.

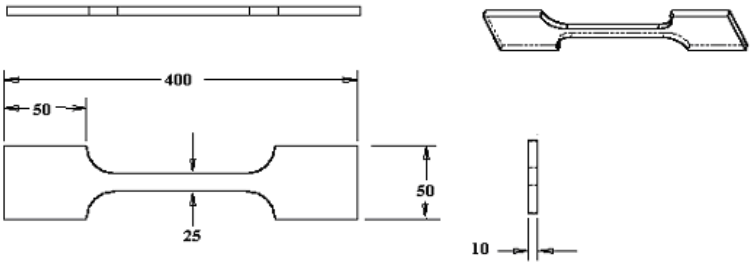

Figure 1: Tensile specimen, all dimensions are in mm

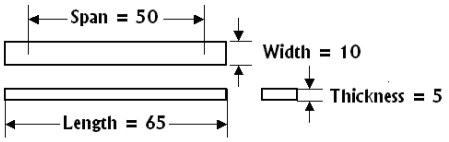

Figure 2: Bending specimen, all dimensions are in mm

2.3. Tests

The heat-treated samples were machined to get specimens for tensile and bending tests. The shape and dimensions of the tensile specimen are shown in figure 1. The computer-interfaced UTM (Universal Testing Machine) was used for the tensile test. The specimens were loaded hydraulically. The loads at which the specimen has reached the yield point and broken were noted down. The extensometer was used to measure the elongation. Three-point bending test was carried out to find flexural strength of the composites. The shape and dimensions of bending specimen are shown in figure 2. Three samples were used for each trial.
The flexural strength was found from the following relation

$$\text{Flexural strength} = \frac{3gPL}{2bt^2}, \text{ Mpa} \qquad (1)$$

where, P is the applied load, l is the span, b is the width, t is the thickness, and g is the acceleration due to gravity.

Hardness data was obtained from the Vickers hardness tester. A load of 10 kg was applied on the square-based diamond-pyramid indenter. The length of the diagonal of the impression was measured through a microscope fitted with an ocular micrometer. Three readings were taken at random locations on the both sides of the specimen. The average value of hardness values was calculated.

2.4. Tests

Microstructures of as-cast and heat treated aluminum composite samples were examined metallographically. The photographs of samples were taken. Samples were firstly cut and mounted. Then they were grinded, polished and etched with Keller solution which contains 1.5% HCl, 2.5% HNO_3, 1% HF, and 95% H_2O.

2.5. Scanning and Transmission Electron Microscopic Analysis

Fracture surfaces of the deformed/fractured (under tensile loading) test samples were examined in a scanning electron microscope (SEM) to determine the macroscopic fracture mode and to characterize the fine-scale topography and establish the microscopic mechanisms governing fracture. Samples for SEM observation were obtained from the tested specimens by sectioning parallel to the fracture surface and the scanning was carried in IICT (Indian Institute of Chemical Technology - Hyderabad) S-3000N Toshiba. The grain boundary structure was also revealed in a transmission electron microscope (TEM).

2.6. X-Ray Structure Analysis

The second phases that may form during casting and heat-treatment were revealed by x-ray structure analysis. X-ray analysis was made by 100 kV Philips twin tube X-ray diffractometer.

3. Results and Discussion

The average values of yield strength, fracture strength, ductility in terms of tensile elongation, and flexural strength are presented in the graphical forms.

3.1 Undeformed Microstructure

The optical micrographs illustrating the microstructures of heat-treated 7072 Al alloy and the as-cast and heat-treated 7072 Al/Al_2O_3 particulate metal matrix composites are shown in figures 3-5. The alloy 7072 Al structure consists of fine and coarse particles of $MgZn_2$ (black) and a few insoluble particles of $FeAl_3$ (light gray) in the aluminum-rich solid solution (figure 3). Figures 4-5 show the random distribution of Al_2O_3 reinforcement particles in the 7072 alloy. The as-cast microstructure (figure 4) reveals coarse grain structure whereas the heat-treated microstructure (figure 5) represents the fine grain structure. At regular intervals, a clustering or agglomeration of Al_2O_3 of varying sizes in high volume fraction composites is observed resulting in Al_2O_3-rich and Al_2O_3-depleted regions (figure 6).

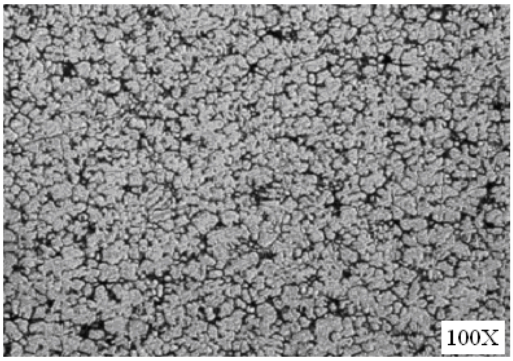

Figure 3: Microstructure of heat-treated 7072Al matrix alloy

X-ray diffractograms of heat-treated 7072 Al/Al_2O_3 (20% V_f) composite is shown in figures 7-8. The microstructure consists of Al_7Cu_2Fe (clustered in bands) and a few Al7Cu2Fe with Si containing particles (figure 7). This phase is precipitated in interdendritic areas. $Mg_{17}Al_{12}$ intermetallic phase is also revealed at the grain boundary junctions (figure 8). TEM microstructure shown in figure 9 reveals that the grain boundary precipitates are found to be coarse and connected. The grain boundary precipitates are mainly particles having the chemistry of $MgZn_2$ (figure 10).

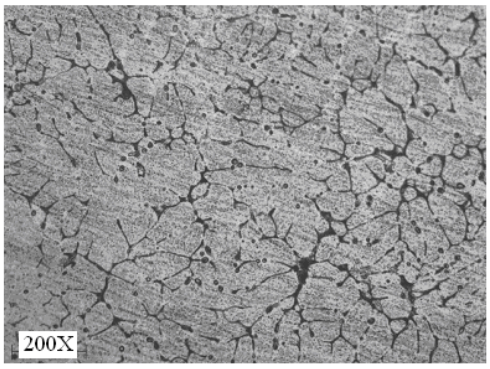

Figure 4: Microstructure of 7072 Al/Al_2O_3 as-cast composite (V_f = 20%)

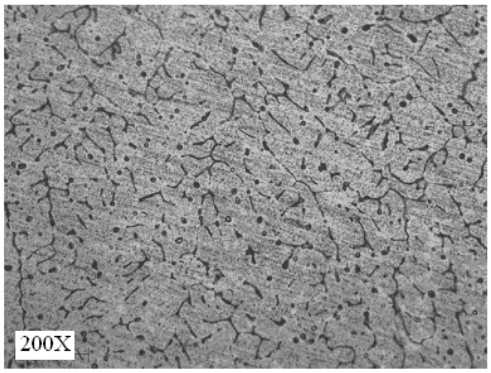

Figure 5: Microstructure of 7072 Al/Al_2O_3 heat-treated composite (V_f = 20%)

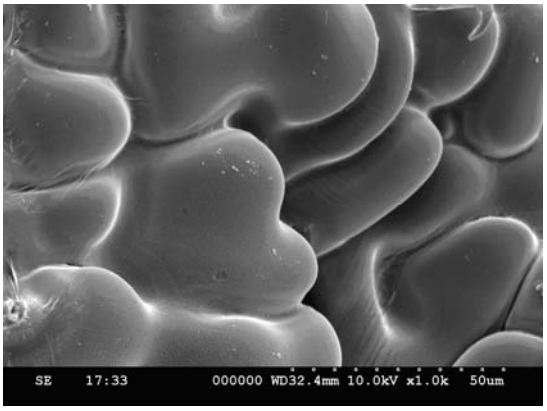

Figure 6: Clustering or agglomeration of Al_2O_3 observed in 7072 Al/Al_2O_3 (V_f = 30%)

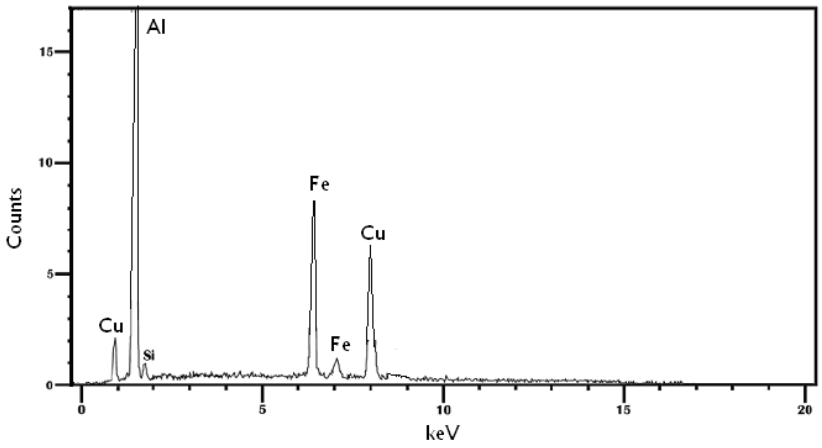

Figure 7: X-ray diffractogram of heat-treated 7072 Al/Al_2O_3 (20% V_f) composite

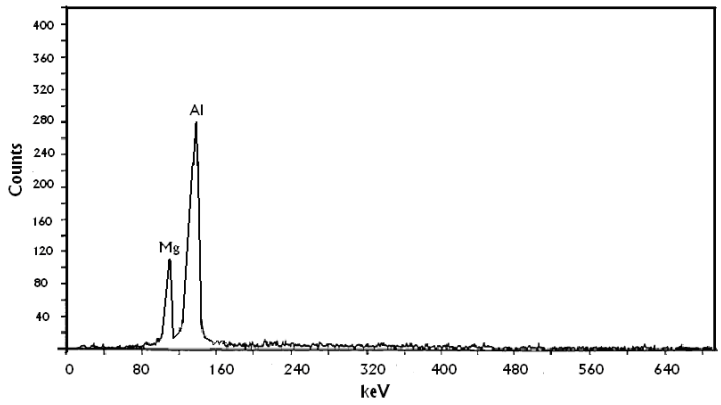

Figure 8: X-ray diffractogram of heat-treated 7072 Al/Al_2O_3 (20% V_f) composite

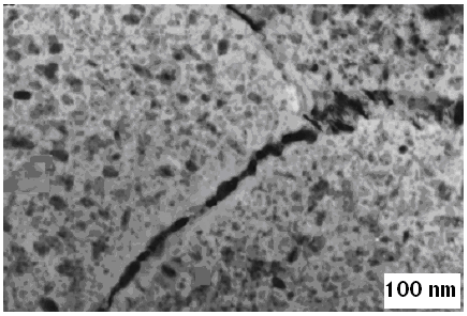

Figure 9: TEM micrographs of heat-treated 7072 Al alloy showing coarse precipitates in the matrix and broken network of coarse grain boundary precipitates

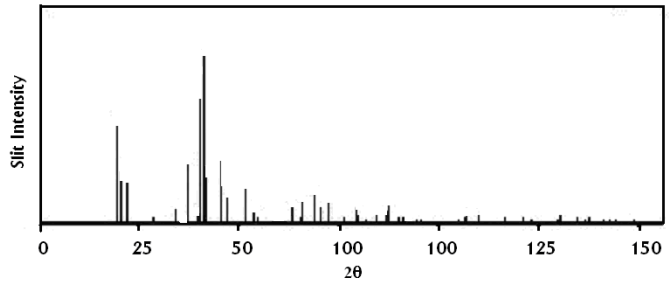

Figure 10: X-ray analysis to recognize second-phase, $MgZn_2$

3.2. Strengthening Mechanisms

The strength of 7072 Al/Al_2O_3 particulate composite is influenced by the following factors:

- Thermal mismatch during heat treatment
- Strain hardening
- Changes in grain size

Thermal expansion mismatch between reinforcing Al_2O_3 particles and 7072 Al matrix alloy can result in internal stresses during heat treatment and tensile testing. Arsenault and Shi (1991) developed a model to quantify the degree of dislocation punching that takes place due to thermal mismatch between the reinforcing particle and matrix. The dislocation density generated due to the thermal mismatch is given by:

$$\rho = 12\Delta T \frac{\Delta C V_p}{bd} \tag{2}$$

where b is the Burger's vector, d is the diameter of the reinforcing particle, V_p is the particle volume fraction, ΔT is the temperature difference, and ΔC is the difference in coefficient of thermal expansion between the particle and matrix. The increase in strength due to dislocation punching is given by:

$$\Delta\sigma_t = k_t G b \rho^{1/2} \tag{3}$$

where k_t is a constant, and G is the shear modulus. The influence of volume fraction on the thermal mismatch-induced stress due age hardening is shown in figure 11. The thermal mismatch-induced stress increases with increase in volume fraction of reinforcing Al_2O_3 particles.

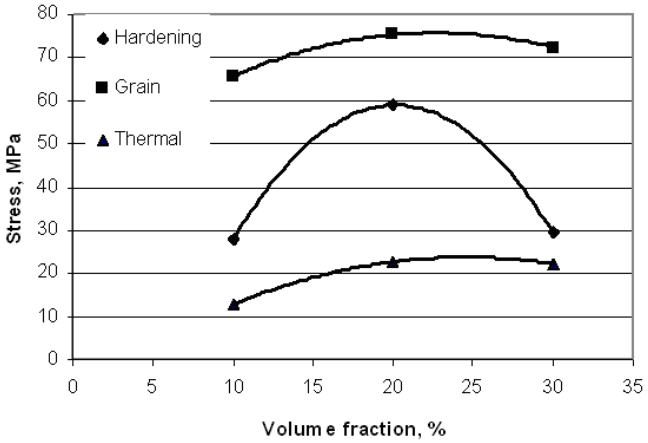

Figure 11: Contribution of different strengthening mechanisms to the yield strength

The yield strength contribution due to changes in the grain size (analogue Hall-Petch) is given by

$$\Delta\sigma_g = k_g D^{-1/2} \tag{4}$$

with $$D = d\left(\frac{1-V_p}{V_p}\right)^{1/3} \tag{5}$$

where D is the resulting grain size, V_p is the particle volume fraction, and K_g is a constant. The grains undergo change in size due to recrystallization during thermo-mechanical treatment of the composite. The increase in yield strength increases with the volume fraction of reinforcing Al_2O_3 due to change in grain size (figure 11). The contribution of change in the grain size is higher than that because of strain hardening and thermal mismatch.

The yield strength is measured the stress with 0.2% remaining elongation. A significant strain hardening occurs, which is dependent on the size of reinforcing particle and its content in the composite as observed by Kelly and Davies (1965). The strain hardening contribution to the yield strength is given by

$$\Delta\sigma_s = k_s GVp\left(\frac{2b}{d}\right)^{1/2} \varepsilon^{1/2} \tag{6}$$

where k_s is a constant, G is the shear modulus, V_p is the volume fraction of reinforcing particle, b is the Burgers vector, d is the reinforcing particle diameter, and ε is the elongation. The strain hardening increases with increase in volume fraction of Al_2O_3 up to 20% (figure 11). Beyond 20% Al_2O_3, the strain hardening decreases due to decrease in elongation of the 7072 Al/Al_2O_3 composite.

3.3. Mechanical Properties

Although tensile testing is not recommended in examining the fracture behavior of Al_2O_3 reinforced aluminum composite, tensile tests were performed to find out yield strength and fracture strength values. However, specimens fractured in the early stages of tensile tests and lower strength values were obtained. Clustering of Al_2O_3 particulates was observed in some of the tensile test specimens. Usually three point bending tests were applied instead of tensile testing in investigating of particulate reinforced metal composites. The main reason is the Al_2O_3 particulates make notch effect during the testing because of machining scratches on the 7072 Al/Al_2O_3 samples.

The variations of yield strength, fracture strength, and flexural strength with volume fraction of Al_2O_3 are shown in figure 12. The yield, fracture, and flexural strengths of heat-treated 7072 Al/Al_2O_3 composite (V_f = 20%) are found to be high. As the volume fraction of Al_2O_3 particles increases beyond 20%, the yield, fracture, and flexural strengths decrease. Composites failed at small strain values during the tensile and bending tests for composites reinforced with 30%Al_2O_3. The matrixes probably did not have enough internal ductility and could not overcome the localized internal stresses. Therefore, the composites failed before reaching the fracture strength of 20% Al_2O_3 composite. All specimens show brittle fracture at macro scale fracture surface examinations. The decrease in the yield, fracture, and flexural strengths is also due to the formation of clusters

of Al_2O_3 in the composite at high volume fractions of Al_2O_3. The precipitated phases, which present along the grain boundaries and in the interdendritic areas are responsible for the initiation and propagation of failure at tensile test. The fracture strength is only marginally higher than the yield strength. The theoretical yield strength is greater than that found by the experiments (figure 13). The reason could be the inhomogeneous distribution of reinforcement and degree of clustering which could reduce the effective amount of particulates for strengthening. The variation in the fracture strength 7072 Al/Al_2O_3 composites is largely affected by the work hardening rate. The flexural strength is superior to both the yield and fracture strengths.

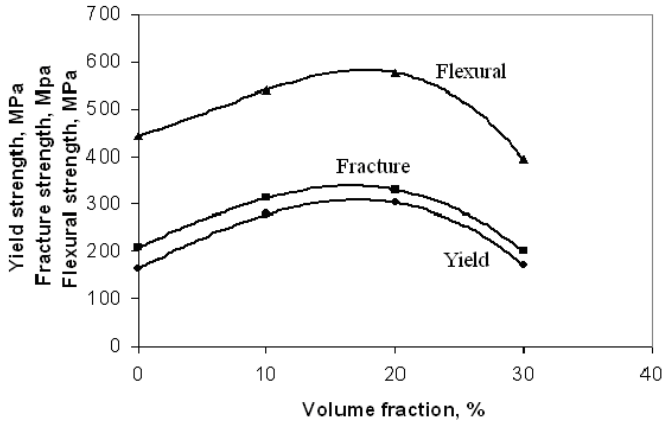

Figure 12: Variation of the yield, fracture, and flexural strengths with the volume fraction of Al_2O_3

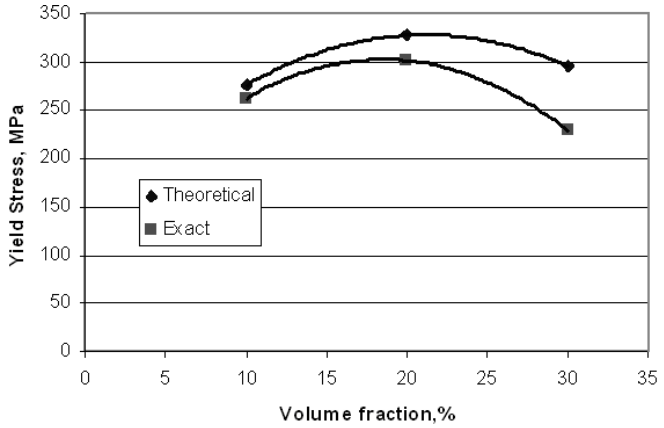

Figure 13: Comparison of theoretically calculated yield strength with the experimentally determined values

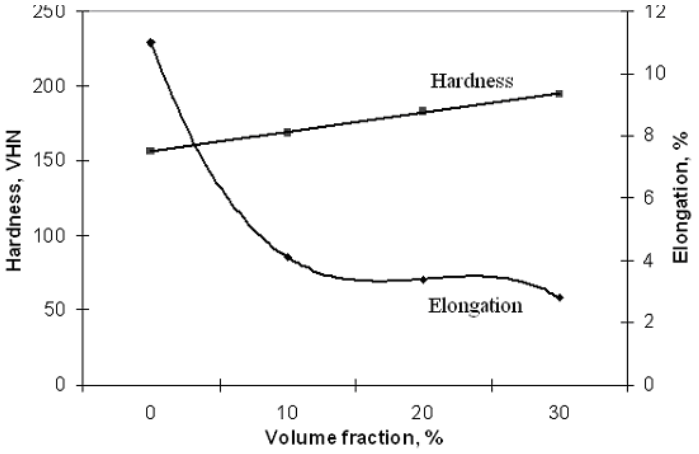

Figure 14: Variation of the ductility and hardness with the volume fraction of Al_2O_3

The influence of volume fraction of Al_2O_3 on the ductility (measured in terms of tensile elongation) and hardness is shown in figure 14. It can be seen that the tensile elongation decreases with increase in volume fraction of Al_2O_3 whereas the hardness increases with increase in volume fraction of Al_2O_3. The decrease in the

ductility can be attributed to the beginning of void nucleation in advance with increasing amount of Al_2O_3 reinforcement and the stress concentrations at reinforcement particles and reaction/precipitated second-phases. Llorca et al (1991) have verified that the microplasticity took place in the metal matrix composites due to stress concentrations in the matrix at the poles of the reinforcement and/or at sharp corners of the reinforcing particles [13]. The increase in hardness may be due to the second-phases precipitated during the heat-treatment of the composites. The second-phases are brittle and hard.

The upper and lower limits of elastic modulus of the composite is found from the rule of mixture (ROM) as follows:

For upper limit, Elastic modulus of the composite, $E_{cu} = E_p V_p + E_m V_m$ (7)

For lower limit, Elastic modulus of the composite, $E_{cl} = \dfrac{E_p E_m}{E_p V_m + E_m V_p}$ (8)

where V_p is the volume percentage of SiC particulate, V_m is the volume percentage of matrix, E_p is the elastic modulus of SiC particulate, and E_m is the elastic modulus of matrix. From the literature, elastic modulus of 7072 Al matrix alloy was found be 68.0 GPa and the manufacturer firm states the elastic modulus of Al_2O_3 as 350 GPa. The elastic modulus was also determined considering the geometry and the orientation of the reinforcement based on the Tsai-Halpin model as follows:

$$E_c = \frac{E_m(1+2sqV_p}{1-qV_p} \tag{9}$$

with $$q = \frac{\frac{E_p}{E_m}-1}{\frac{E_p}{E_m}+2s} \tag{10}$$

where s is the aspect ratio of the reinforcing particles. Theoretically, elastic modulus increases with increase in the volume fraction of Al_2O_3 as shown in figure 15. The elastic modulus determined based on the Tsai-Halpin model is more accurate than that calculated by the ROM.

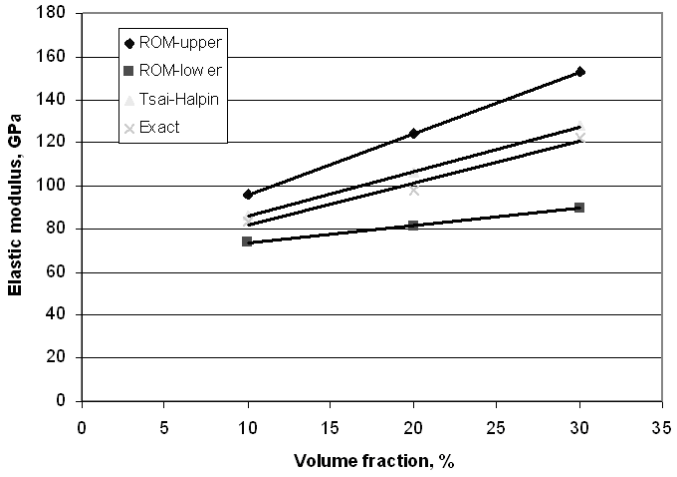

Figure 15: Variation of elastic modulus with volume fraction of Al_2O_3

4. Fracture Behavior

The tensile fracture behavior of heat-treated 7072 Al/Al_2O_3 metal matrix composites, which were cast by the gravity die casting process were studied in the present work. Examination of the tensile fracture surfaces (figures 16-18) reveals features fragrant of locally ductile and brittle mechanisms. The factors influencing the ductile and brittle fracture are the non-uniform distribution of Al_2O_3 particles in the 7072 aluminum alloy metal-matrix (figure 5), and the formation of second-phases along the grain boundaries (figure 9) and in the indendritic regions during the casting and heat-treatment. Failures of 7072 Al/Al_2O_3 composites are because of void nucleation at particle/matrix interfaces (figure 16), decohesion of particles from the matrix (figure 17), and particle/cluster cracking (figure 18).

The mismatch due to the difference in the strain carrying capability between the hard reinforcement Al_2O_3 promotes stress concentrations near the reinforcement Al_2O_3 and second-phases. This situation generates favorable conditions for the Al_2O_3 particles, second-phases (reaction compounds and intermetallics) and clusters to crack and subsequently the decohesion of Al_2O_3 particles from the adjacent matrix alloy (figure 17). Simultaneous failure of the reinforcement Al_2O_3, second-phase particles in the composite microstructure is governed by the contending influences of the local plastic constraints, and the degree of clustering (figure 18). Koss and Copley (1971) have reported that the local plastic constraints were particularly important for the larger-sized particles and particle clusters during composite fracture. Secondly, the mismatch due to differences in the coefficient of thermal expansion between the Al_2O_3 particles, the 7072 aluminum alloy matrix, and the precipitated phases induces dimple micro structure in the composite. The presence of Al_2O_3 reinforcement particles reduces the average distance in the composite by providing strong barriers to the dislocation motion. The interaction of dislocations with other dislocations, precipitates, and Al_2O_3 particles causes the dislocation motion. Residual dislocation loops are left around each particle after a dislocation passes the particles. The dislocation motion results in dimple structure (figure 16).

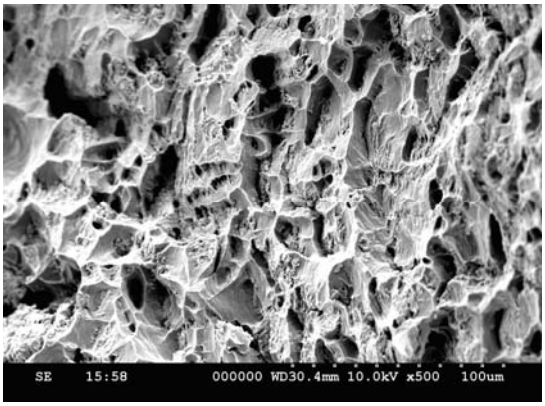

Figure 16: SEM of fracture surface of heat-treated fatigue sample (V_f = 10%)

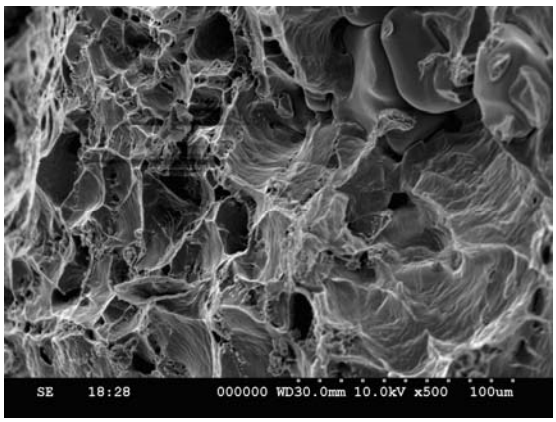

Figure 17: SEM of fracture surface of heat-treated fatigue sample (V_f = 20%)

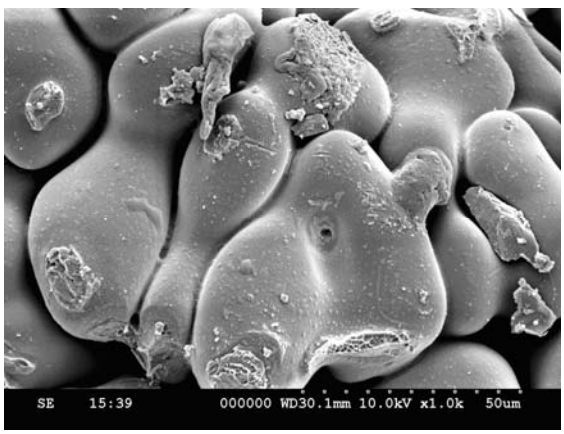

Figure 18: SEM of fracture surface of heat-treated fatigue sample (V_f = 30%)

Srivatsan and Hajri, (2002) have reported that the void nucleation occurs at particle/matrix interfaces and can be realized by either interface decohesion or particle cracking. The microscopic voids are associated with failure of the ductile metal matrix between the reinforcement particles, whereas the macroscopic voids are coupled with the reinforcement Al_2O_3. The sources of macroscopic voids and resultant shallow dimples on the fracture surface are the critical events controlling both the fracture and decohesion of the reinforcement Al_2O_3 particles (figure 16). The constraints induced by the presence of hard and brittle alumina particle reinforcements in the soft and ductile 7072 metal-matrix. The voids then grow under both the applied load and the influence of local plastic constraint until a coalescence mechanism is activated, and this followed by the total failure of the specimen. The void coalescence occurs when the void elongates to the initial intervoid spacing. This leads to the dimpled appearance of the fractured surfaces (figure 16). During the later stages of deformation, microscopic cracks initiate and grow in the region of high plasticity and aided by the local elevation of hydrostatic stresses due to the presence of coarse Al_2O_3 particles. This confirms the important role played by the local plastic strains in governing damage initiation and propagation in the 7072 Al/Al_2O_3 composite microstructure. The fracture due to tensile loading is ductile and brittle in nature.

Preferential dissolution of $MgZn_2$ precipitates assisted by its continuous nature along the grain boundary makes the grain boundary an easy path for the crack growth (figure 9). Clusters of particles evident on the fracture surface were found to contain Al, Cu, and Fe through EDS analysis (figure 7). These are coarse constituent phase particles, Al_7Cu_2Fe. Their presence on the fracture surface suggests that they precipitate at the boundaries, contribute to stress concentrations, and promote development of microcracks. During heat treatment at chosen temperature, there occurs partial dissolution of minority phases. Homogenization of microstructure is accompanied by simultaneous forming of intergranular nonintegrities, which is unfavourable from the viewpoint of strength and plastic properties. Beside the dislocation motions due to thermal mismatch, the possibility of the cross-slip of screw dislocations and/or climb of edge dislocations can also be taken into account as the mechanisms responsible for the fracture mechanism of the composites.

5. Conclusions

In tensile and bending tests, the composites having volume fraction of 20% alumina gave the maximum strength. The flexural, fracture and yield strengths decreased with increase in volume fraction of Al_2O_3 beyond 20%. The strengthening mechanisms were largely governed by the strain hardening and by the change in grain size. The hardness increased with the increase of alumina addition to 7072 Al matrix alloy. The ductility decreased with the increase in volume fraction of Al_2O_3 in the composite. Clustering/agglomeration of alumina particulates was observed in some of the tensile test specimens. Heat-treated composites were examined with x-ray analysis to find precipitated phases. The coarse and connected $MgZn_2$ phases were precipitated along the grain boundaries. $Mg_{17}Al_{12}$ intermetallic phase was also revealed at the grain boundary junctions. Al_7Cu_2Fe were clustered in bands in the composite. The tensile fracture was governed by the ductile and brittle behaviors because of void nucleation at particle/matrix interfaces, decohesion of particles from the matrix and particle/cluster cracking.

Acknowledgements

The author acknowledges with thanks All India Council for Technical Education (AICTE) – New Delhi for sectioning R&D project, and Indian Institute of Chemical Technology – Hyderabad for their technical help.

References

[1] Arsenault, R.J. (1984): The strengthening of aluminum 6061 by fiber and platelet silicon carbide. Materials Science and Engineering, 64, pp.171-181.
[2] Arsenault, R.J.; Shi, N.; Feng, C.R.; Lang, L. (1991): Strengthening of composites due to microstructural changes in the matrix. Acta Metallurgica, 39, pp.47-57.
[3] Chawla, K.K. (1997): *Composite materials: Science and Engineering*. 2nd edn, Press: Springer-Verlag, New York, pp.102-104.
[4] Dutta, L.; Bourell, D.L. (1990): Influence of dislocation density and distribution on the aging behavior of 6061 Al-SiC composites. Acta Metallurgica, 38, pp.1990-2041.
[5] Hunt, W.H.; Cook, C.R.; Sawtell, R.R. (1991): Cost effective high performance powder metallurgy aluminum matrix composites for automotive applications. Annual SAE Congress, paper No. 910834, Detroit, Michigan.
[6] Kelly, A.; Davies, D.J. (1965): The principles of the fiber reinforcement of metals. Metallurgical Reviews, 10, pp.1–78.
[7] Koss, D.A.; Copley, S.M. (1971): Thermally-induced residual stresses in eutectic composites. Metallurgical Transactions, 2, pp.1557–60.
[8] Llorca, J.; Needleman, A.; Suresh, S. (1991): An Analysis of the Effects of Matrix Void Growth on Deformation and Ductility in Metal-Ceramic Composites. Acta Metallurgica, 39, pp.2317-2335.
[9] Lloyd, D.J. (1991): Aspects of fracture in particulate reinforced metal matrix composites. Acta Metallurgica, 39(1), pp.59-71.
[10] Nair, S.V.; Tien, J.K.; Bates, R.C. (1985): SiC reinforced aluminum metal matrix composites. International Materials Reviews, 30(6), pp.275-290.

[11] Srivatsan, T.S.; Ibrahim, I.A.; Mohamed, F.A.; Laverna, E.J. (1991): Processing techniques for particulate reinforced metal aluminum matrix composites. Journal of Materials Science, 26, pp.5965-5978.
[12] Srivatsan, T.S.; Al-Hajri, M.(2002): The Fatigue and final fracture behavior of SiC particle reinforced 7034 aluminum matrix composites. Composites Part B, 33, pp.391-404.
[13] Wang, Z.; Zhang, R.J. (1991): Mechanical behavior of cast particulate SiC/Al (A356) metal matrix composites. Metallurgical Transactions, 22A, pp. 1585-1593.
[14] Youssef, Y.M.; Dashwood, R.J.; Lee, P.D. (2005): Effect of clustering on particle pushing and solidification behavior in TiB_2 reinforced aluminum PMMCs. Composites Part A, 36, pp.747-763.
[15] Zhou, W.; Xu, Z.M. (1997): Casting of SiC reinforced metal matrix composites. Journal of Materials Processing Technology, 63, pp.358-363.rix composites. Composites Part B, 33, pp.391-404.